Beiträge zur Tabakforschung International
Contributions to Tobacco Research
Volume 28 · No. · August 2018
DOI: 10.2478/cttr-2018-0007

Theoretical and Experimental Analysis of the Metal-Based Ignition Propensity Test Thermodynamics *

by

Pablo Guindos [1,2], Apurva Patel [3], and Minia-Xisela Rodriguez [4]

[1] Pontificia Universidad Católica de Chile, 7820436 Santiago, Chile
[2] Centro UC de Innovación en Madera, 7820436 Santiago, Chile
[3] Technische Universität Braunschweig, 38104 Braunschweig, Germany
[4] Dictuc S.A., 7820436 Santiago, Chile

SUMMARY

This research analysed in detail the performance of the new alternative ignition propensity test prescribed in the standard ASTM E2187-16, which is based on the utilization of a substrate comprising a thin steel plate along with one filter paper. The analysis was performed both experimentally, by means of infrared temperature measurements, and theoretically by using a comprehensive finite element model that was able to predict the temperature of the substrate with errors of only 7.3% and 15.7% in space and time, respectively. While the new alternative test was able to reduce the variability of the heat absorbance from 33% to only 4% with respect to the conventional tests, it showed several downsides that critically reduce its reliability. The heat absorbance of the alternative test did not correctly emulate the conventional procedure as it absorbed as much heat as twice. The gravity effect on the plate increased the air gap thickness more than twice, thereby decreasing potentially the heat absorbance by 13%. In addition, a mechanical analysis showed that compressive stresses due to high temperature gradients could cause irreversible buckling, creep and yielding of the plate. Experiments showed that in fact the concavity of the plate was prone to increase after testing. Assuming the maximum concavity allowed by the standards, the heat absorbance was halved in respect to a perfectly flat plate. In view of these results, the utilization of the conventional test method still appears clearly more appropriate than the alternative one. [Beitr. Tabakforsch. Int. 28 (2018) 52–64]

ZUSAMMENFASSUNG

Diese Untersuchung analysierte die Leistung des neuen, alternativen Zündneigungstests. Er ist im Standard ASTM E2187-16 beschrieben und basiert auf der Verwendung eines Substrats, das eine dünne Stahlplatte zusammen mit einem Filterpapier umfasst. Die Analyse wurde sowohl experimentell mittels Infrarot-Temperaturmessungen als auch theoretisch unter Verwendung eines umfassenden Finite-Elemente-Modells durchgeführt; dieses konnte die Temperatur des Substrats in räumlicher Richtung mit Fehlern von nur 7.3% und im zeitlichen Verhalten von 15.7% vorhersagen. Der hier vorgestellte Test ist in der Lage, die Variabilität der Wärmeabsorption von 33% auf nur 4% gegenüber dem herkömmlichen Test zu reduzieren. Er weist jedoch auch einige Nachteile auf, die seine Zuverlässigkeit erheblich reduzieren, da die Wärmeabsorption beim neuen Verfahren doppelt so hoch ist wie beim herkömmlichen Verfahren. Die Wirkung der Schwerkraft auf die Platte erhöht die Dicke des Luftspalts auf mehr als das Doppelte, wodurch sich die Wärmeabsorption um 13% verringert. Darüber hinaus zeigte eine mechanische Analyse, dass Druckspannungen aufgrund von hohen Temperaturgradienten ein irreversibles Wölben, Kriechen und Verformen der Platten verursachen können. Experimente zeigen, dass die Konkavität der Platte nach dem Testen ansteigt. Bei der im Standard maximal erlaubten Konkavität ist die Wärmeabsorption gegenüber einer vollkommen flachen Platte halb so groß. In Anbetracht dieser Ergebnisse ist der herkömmliche Test der neuen Alternative vorzuziehen. [Beitr. Tabakforsch.Int. 28 (2018) 52–64]

*Received: 11th January 2018 – accepted: 17th May 2018

RESUME

La présente étude analyse, dans le menu détail, les performances du nouveau test alternatif de la propension à l'inflammation prescrit dans l'ASTM E2187-16; ce test s'appuie sur l'utilisation d'un substrat composé d'une fine plaque d'acier et d'un papier-filtre. L'étude est réalisée, à la fois, suivant une approche expérimentale au travers de relevés de température par infrarouge et de façon théorique grâce à un modèle complet à éléments finis, qui nous a permis de prédire la température du substrat avec de faibles taux d'erreur de respectivement 7,3% et 15,7% dans l'espace et dans le temps. Bien que le nouveau test alternatif permette de réduire la variabilité de l'absorption thermique de 33% à seulement 4% comparativement aux tests conventionnels, il présente aussi plusieurs inconvénients qui nuisent gravement à sa fiabilité. L'absorption thermique du test alternatif ne reproduit pas exactement la procédure conventionnelle car le test absorbe deux fois plus de chaleur que cette dernière. L'effet de la gravité sur la plaque fait plus que doubler l'épaisseur de la couche d'air et réduit ainsi potentiellement l'absorption thermique de 13%. En outre, une analyse mécanique démontre que les contraintes de compression liées aux importants gradients de température pourraient provoquer des effets irréversibles tels qu'un gondolement, un fluage et une déformation de la plaque. Les expériences démontrent qu'en fait, la concavité de la plaque est susceptible d'augmenter à l'issue du test. A la concavité maximale autorisée par les normes, l'absorption thermique est divisée par deux par rapport à celle d'une plaque parfaitement plate. Au vu de ces résultats, la méthode de test conventionnelle semble toujours clairement mieux convenir que l'approche alternative. [Beitr. Tabakforsch. Int. 28 (2018) 52–64]

NOMENCLATURE

Letters

A	Pre-exponential factor (*1/s*)
C	Elasticity tensor (*Pa*)
c	Specific heat capacity (*J/kgK*)
d	Thickness (*m*)
D	Diffusion coefficient (m^2/s)
E	Activation energy (*J/mol*) or Young's Modulus (*Pa*)
F_V	Volumetric force (N/m^3)
g	Gravitational acceleration (m/s^2)
h	Enthalpy (*J/kg*) or convective heat transfer coefficient (W/m^2K)
ΔH	Heat of the reaction (*J/kg*)
K	Permeability (m^2)
k	Thermal conductivity (*W/mK*)
M	Molecular mass (*kg/mol*)
$\dot{m}''$	Mass flux (kg/m^2s)
n_{cp}	Exponential factor of the specific heat equation (nd = no dimension)
n	Substrate's surface normal (nd)
P	Pressure (*Pa*)
Q'''	Volumetric rate of heat source (W/m^3)
$\dot{q}''$	Heat flux (W/m^2)
r	Cigarette's radius (*m*)
R	Universal gas constant (*J/mol K*)
t	Time (*s*)
T	Temperature (*K*)
u	Velocity vector (*m/s*) or displacement (*m*)
v	Burning rate of the cigarette (*m/s*) or Poisson's ratio (nd)
x	Parallel to the cigarette substrate's coordinate (*m*)
X	Volume fraction (*%*)
y	Transverse to the cigarette substrate's coordinate (*m*)
Y	Mass fraction (*%*)
z	Substrate's depth coordinate (*m*)

Greek symbols

α	Thermal expansion coefficient (*1/K*)
γ_T	Cigarette's temperature reduction factor (nd)
δ	Thickness (*m*)
ρ	Density (kg/m^3)
ε	Emissivity (nd) or strain (nd)
κ	Permeance ($m/Pa \cdot s$)
μ	Dynamic viscosity ($Pa \cdot s$)
ν	Kinematic viscosity (m^2/s)
σ	Stefan-Boltzmann constant (W/m^2K4) or stress (*Pa*)
Ψ	Porosity (nd)
$\dot{\omega}'''$	Volumetric reaction rate (kg/m^3s)

Subscripts

air	Air gap
amb	Ambient
cell	Cellulose (dry filter paper)
ch	Char
cig	Cigarette
cs	From the cigarette to the substrate
chox	Char oxidation reaction
d	Destruction of species
ef	Effective value
el	Elastic
ev	Evaporation reaction
f	Formation of species
g	Total gas
i	Condensed species index: cell, m, ch
j	Gas species index:N2, O2, vap, pgas
k	Reaction index: ev, pyr
l	Lower side of the substrate
m	Moist filter paper
N2	Nitrogen
O2	Oxygen
0	Initial
p	At constant pressure
pgas	Pyrolysis gases (pyrolysates)
pyr	Pyrolysis reaction
s	Solid non-porous density
steel	Steel plate
th	Thermal
u	Upper side of the substrate
vap	Water vapor

Superscripts

Weighted or averaged value

INTRODUCTION

Recently, an alternative testing method to assess the ignition propensity (IP) of cigarettes has been prescribed in ASTM E2187-16 (1). In essence, this new test consists of placing a conventional cigarette on a substrate composed of one upper layer of filter paper Whatman® No. 2 and one lower layer of full-hard stainless steel 302 to determine whether the cigarette can self-extinguish or not. If the cigarette self-extinguishes during such a metal-based ignition propensity test (MIPT), it can be assumed that the risk is lower for a cigarette to cause potential damage when mistakenly left unattended in a typical worst-case scenario, such as smouldering when dropped onto couches or similar furniture.

The new MIPT method serves as alternative to the conventional ignition propensity test, which applies not only in the United States of America by means of the ASTM E2187-16, but also at the international level by the ISO 12863 (2) which has been developed based on the ASTM E2187-09. The basis of the conventional cellulose-based ignition propensity test (CIPT) is the same as MIPT except that the thin steel lower plate is replaced by 9 further layers of Whatman® paper No. 2, thus forming in total a stack of 10 filter paper layers.

A major reason for establishing such an alternative as MIPT is because of the high costs, large variability and high complexity of the CIPT, namely the smouldering process of cellulose and the uneven flatness of the distinct layers (3). In fact, the CIPT has already been studied from both the stochastic (4–7) and theoretical point of view (3, 8) with different levels of complexity. Sophisticated models have revealed that, regarding the substrate, the thickness of the air gap between the 10 layers of the filter paper, the heat capacity and pyrolysis activation energy govern the overall variability of the test (3). While the first two parameters may not be critical, because one usually does not expect high variability of heat capacity and activation energy, the air gap thickness becomes less controllable. This is because the paper deforms during the conditioning phase due to natural shrinking and swelling, as well as due to the manipulation necessary to set up the test. Even when intuition suggests that those deformations are very small, the low thickness of one filter paper, along with the distinct thermal properties of air and cellulose produce considerable differences on the heat absorbed by a deformed paper in comparison to a perfectly flat substrate (3). In addition, the weight of the substrate and cigarette also cause uneven distribution of air gap thickness, thus further increasing the variability of the test (3). Therefore, it seems quite challenging to decrease the variability of the CIPT.

As stated by MITLER and WALTON (9), a given substrate influences the IP in three different ways. The first and more obvious reason is that the substrate absorbs some part of the heat released by the cigarette. The more the heat is absorbed, the more likely the self-extinguishment becomes. Thus, a thicker and more conductive substrate is more prone to induce cigarette extinguishment because it absorbs a larger quantity of heat. The second reason, which actually indirectly influences the first, is related to the chemical reactions happening in the substrate during thermal degradation. If reactions are very endothermic, the cigarette is much more likely to cause extinguishment. Research has shown that pyrolysis is a relatively 'neutral' reaction in that it is not largely endo- or exothermic, and char oxidation, even though it is very exothermic, only develops to a small extent because of the low temperatures (3). Thus, evaporation may be considered as the most important reaction in terms of cigarette's heat absorption. Finally, the third reason is that the substrate acts as a barrier for the oxygen to penetrate through and supports the oxidative chemical reactions on the cigarette. The less permeable the substrate is, the more difficult it is for oxygen to diffuse to the cigarette and thus extinguishment becomes more likely. However, as stated by MITLER and WALTON the influence of an airtight substrate is minor, because the largest part of oxygen consumed by the smouldering tobacco column arrives from sides and top air of the cigarette (9).

Given the three influencing factors mentioned above, in principle it is always feasible to test the ignition propensity (IP) of a cigarette with various types of substrates, including airtight inorganic materials. In addition, the presence of only one air gap in the MIPT should significantly decrease test variability as homogeneity is expected to be much better than that of the 10-layer-scenario of the CIPT. Consequently, the MIPT is feasible and may improve conventional IP testing.

However, the thermodynamics and experimental details of the CIPT remain rather unknown. While experimental testing has been carried out at several laboratories for including this procedure in the standards (10), the theoretical background and experimental details have not yet been analysed. The objective of this research was to perform a detailed theoretical and experimental analysis as conducted for the CIPT (3) in order to determine the effectivity of the new test against the conventional procedure as well as to identify the key parameters governing the thermodynamics of this alternative test.

NUMERICAL MODEL

The thermodynamics underlying the thermal response of a smouldering filter paper are much more complicated than the response of the steel plate. This is because the latter is a non-charring and nonporous solid, i.e., it does not suffer any chemical reaction and heat is transported solely via conduction. Therefore, the model we used is similar to that of the CIPT except that it also includes a nonporous and non-charring solid representing steel. As details of the CIPT model have been presented elsewhere (3), only the fundamentals are outlined in the following.

Governing equations

The core of the model relies on the assumption that solid, condensed and gas phases are conserved, as well as the involved chemical species, the momentum and the energy. The specific equations, along with their meaning are presented in Table 1.

Table 1. Experimental measurements of the cellulosic substrate prior to the elaboration of the mathematical model.

Conserved quantity	Equation	Explanation
Solid phase conservation	$\frac{\partial \bar{\rho}}{\partial t} = -\dot{\omega}'''_{fg}$	*Δ substrate's density = − formation of gases*
Gas phase conservation	$\frac{\partial \left(\rho_g \bar{\psi}\right)}{\partial t} + \frac{\partial \dot{m}''_x}{\partial x} + \frac{\partial \dot{m}''_y}{\partial y} + \frac{\partial \dot{m}''_z}{\partial z} = \dot{\omega}'''_{fg}$	*Δ gas + gas convection = formation of gases*
Condensed phase species conservation	$\frac{\partial \left(\bar{\rho} Y_i\right)}{\partial t} = \dot{\omega}'''_{fi} - \dot{\omega}'''_{di}$	*Δ solid sp. = formation solid sp. − destruction solid sp.*
Energy conservation [a]	$\frac{\partial \left(\overline{\rho h}\right)}{\partial t} = -\frac{\partial \dot{q}''_x}{\partial x} - \frac{\partial \dot{q}''_y}{\partial y} - \frac{\partial \dot{q}''_z}{\partial z} - \dot{m}''_x c_{pg} \frac{\partial T}{\partial x} - \dot{m}''_y c_{pg} \frac{\partial T}{\partial y} - \dot{m}''_z c_{pg} \frac{\partial T}{\partial z} + \sum_k \dot{Q}''' + \sum \left(\dot{\omega}'''_{fi} - \dot{\omega}'''_{di}\right) \cdot h_i$	*Δ enthalpy = − conduction − exchange with gas + reactions sources + change of sensible enthalpy due to formation and destruction of the solid species*
Gas phase momentum (pressure evolution)	$\frac{\partial}{\partial t}\left(\frac{P\overline{M}}{RT}\bar{\psi}\right) = \frac{\partial}{\partial x}\left(\frac{\overline{K}}{v}\frac{\partial P}{\partial x}\right) + \frac{\partial}{\partial y}\left(\frac{\overline{K}}{v}\frac{\partial P}{\partial y}\right) + \frac{\partial}{\partial z}\left(\frac{\overline{K}}{v}\frac{\partial P}{\partial z}\right) + \dot{\omega}'''_{fg} - g_z \frac{\partial}{\partial z}\left(\frac{\overline{K}}{v}\rho_g\right)$	*Δ gas density = variation due to pressure change + formation of gases − variation due to gravity force*

[a] with k = *ev,pyr* and i = *cell, m, ch*

Reactions and heat sources

Both the evaporation and the pyrolysis reactions are taken into account as well as their associated heat. The char oxidation is not accounted for because previous research demonstrated that temperatures on the IP test are not enough for this reaction to completely develop (3). Consequently, air is only modelled as an inert gas phase and oxidation is not accounted for. The different reactions, as well as condensed and gas species implemented in the model are presented in Figure 1. The corresponding equations that are used for modelling each reaction are detailed in Table 2, and the corresponding heat sources are presented in Table 3.

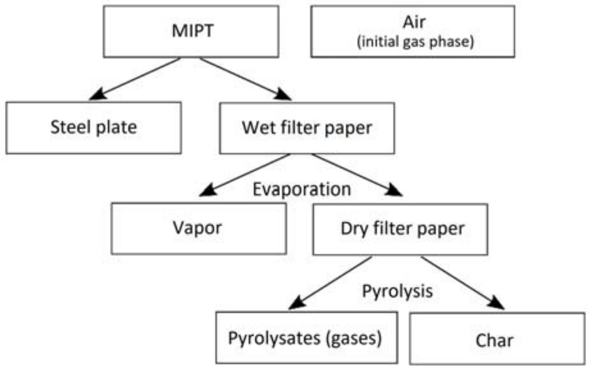

Figure 1. Schematic of the gas species, condensed species and reactions accounted for in the model.

Physical properties

The physical properties are regarded as averaged properties dependent upon the relative importance of each condensed or gas phase species. The summary of the equations used for averaging each property is given in Table 4.

Air gap

The air gap thickness between the filter paper and steel plate is considered with a parabolic equation that reflects the 3D-measurements obtained via laser triangulation (3):

$$d_{air} = \frac{x^2 - y^2}{183.34} + 0.6 \cdot 10^{-4} \qquad [1]$$

where all units are in meters. The modelling of this air gap is accomplished via the classic thin resistive layer such that the air flux through the upper side of the air gap becomes

$$-n_u \cdot \ddot{q}_u = k_{air} \frac{T_l - T_u}{d_{air}} \qquad [2]$$

while heat flux through the lower side of the air gap becomes

$$-n_l \cdot \ddot{q}_l = k_{air} \frac{T_u - T_l}{d_{air}} \qquad [3]$$

Table 2. Equations used for modelling the reactions of the distinct species.

Species	Formation	Destruction
Wet filter paper	—	$\dot{\omega}'''_{dm} = \bar{\rho} Y_m A_{ev} \exp\left(-\frac{E_{ev}}{RT}\right)$
Dry filter paper	$\dot{\omega}'''_{fcell} = \dot{\omega}'''_{dm} \frac{\rho_{cell_0}}{\rho_{m_0}}$	$\dot{\omega}'''_{dcell} = \bar{\rho} Y_{cell} A_{pyr} \exp\left(-\frac{E_{pyr}}{RT}\right)^{n_{pyr}}$
Vapor	$\dot{\omega}'''_{fvap} = \dot{\omega}'''_{dm}\left(1 - \frac{\rho_{cell_0}}{\rho_{m_0}}\right)$	—
Char	$\dot{\omega}'''_{fch} = \dot{\omega}'''_{dcell} \frac{\rho_{ch_0}}{\rho_{cell_0}}$	—
Pyrolysates	$\dot{\omega}'''_{fpgas} = \dot{\omega}'''_{dcell}\left(1 - \frac{\rho_{ch_0}}{\rho_{cell_0}}\right)$	—
Total gas	$\dot{\omega}'''_{fgas} = \dot{\omega}'''_{fv} + \dot{\omega}'''_{fpgas}$	—

Table 3. Heat sources associated with the pyrolysis and evaporation reactions.

Heat source	Equation
Evaporation	$\dot{Q}'''_{ev} = -\dot{\omega}'''_{fvap}\Delta H_{ev}$
Inert pyrolysis	$\dot{Q}'''_{pyr} = -\dot{\omega}'''_{fpgas}\Delta H_{pyr}$

Table 4. Equations used for averaging each physical property according to the relative importance of each species.

Property	Equation
Volume fraction	$X_i = \bar{\rho}\frac{Y_i}{\rho_i}$
Average density	$\bar{\rho} = \left(\sum_{i=1}^{3}\frac{Y_i}{\rho_i}\right)^{-1}$
Porosity	$\psi_i = 1 - \frac{\rho_i}{\rho_{s,i}}$
Average porosity	$\bar{\psi} = \sum_{i=1}^{3} X_i\,\psi_i$
Average thermal conductivity	$\bar{k} = \sum_{i=1}^{3} X_i k_i$
Average heat capacity	$\bar{c}_P = \sum_{i=1}^{3} Y_i c_{pi}$
Average enthalpy	$\bar{h} = \sum_{i=1}^{4} Y_i h_i$
Average emissivity	$\bar{\varepsilon} = \sum_{i=1}^{3} X_i \varepsilon_i$
Average permeability	$\bar{K} = \sum_{i=1}^{3} X_i K_i$
Gas phase density	$\rho_g = \frac{P\bar{M}}{RT}$

This approach made it possible not to explicitly use specific elements for meshing the air gap, which turned out to be very favourable from a computational standpoint.

Boundary and initial conditions

The temperatures of the cigarette (T_{cig}) were taken from the measurements of BAKER (11) by averaging gas and solid phase temperatures as reported in (8). Furthermore, a reduction factor of 0.9 was applied to account for the cooling effect of the substrate on the cigarette (3). The final temperatures considered are presented in Table 5.

Table 5. Cigarette's temperature used as boundary condition.

Distance from cigarette's tip (mm)	Temperature or T_{cig} (K)
0	298
1	312
2	360
3	533
4	687
5	709
6	708
7	684
8	657
9	610
10	579
11	553
12	515
12	298
14	298

The transient (time varying) temperature distribution of the cigarette was taken into account by simply assuming that the tobacco column is aligned with the *x* axis and that the cigarette's tip moves according to the smouldering velocity such as previously published (8)

$$T_{cig}(t) = T_{cig}(x + t \cdot v_{ig}) \qquad [4]$$

A summary of the different boundary conditions considered for solving each conservation equation is presented in Table 6. These boundary conditions are based on those reported by MITLER and WALTON (9).
The initial conditions considered the ambient temperature and pressure, as well as initial density of the solid species. A summary is shown in Table 7.

Material data

Most material data of this model was measured experimentally as detailed in (3). The properties of the 302 full-hard stainless steel are well-known and were obtained from literature (12). The summary of the material data used in this model is presented in the Table 8

Table 6. Summary of the boundary conditions*, based on MITLER and WALTON (9).

Conservation equation	Boundary condition	Application surface	Expression
Momentum (pressure)	Symmetry	Substrate's cross section	$-n \cdot \rho u = 0$
	External pressure	Upper and lower sides	$p = P_{amb}$
Heat	Symmetry	Substrate's cross section	$-n \cdot q = 0$
	Convective heating	Upper side	$-n \cdot q = 71 \cdot \Omega \cdot \left(T_{cig} - T_{amb}\right)$
	Radiative heating	Upper side	$-n \cdot q = \varepsilon_{ef} \cdot \Omega \cdot \sigma \cdot \left({T_{cig}}^4 - {T_{amb}}^4\right)$
	Convective cooling	Upper side	$-n \cdot q = \left(10 + 61 \cdot \Omega\right) \cdot \left(T_{amb} - T_{cig}\right)$
	Radiative cooling	Upper side	$-n \cdot q = \left(\varepsilon_{ef} \cdot \Omega + \bar{\varepsilon} \cdot \left(1 - \Omega\right)\right) \cdot \sigma \cdot \left({T_{cig}}^4 - {T_{amb}}^4\right)$
	Convective cooling	Lower side	$-n \cdot q = 10 \cdot \left(T_{amb} - T\right)$
	Radiative cooling	Lower side	$-n \cdot q = \bar{\varepsilon} \cdot \sigma \cdot \left({T_{amb}}^4 - T^4\right)$
	Outflow	Peripheral surface	$-n \cdot q = 0$

* Ω is the view factor, $\Omega = e^{-y^2/\sigma_y}$ being $\sigma_y = 0.8 \cdot r$ where *r* is the radius of the cigarette and

ε_{ef} is the effective emissivity, i.e., $\varepsilon_{ef} = \dfrac{\varepsilon_{cig} \cdot \bar{\varepsilon}}{1 - \left(\left(1 - \bar{\varepsilon}\right) \cdot \left(1 - \varepsilon_{cig}\right)\right)}$

The numerals 71, 10, and 61 in the heat boundary conditions were proposed by (9).

Table 7. Summary of the initial conditions.

Conservation equation	Initial condition	Application domain	Expression
Momentum (pressure)	Pressure	Filter paper	$P = P_{amb}$
Heat	Temperature	Filter paper and steel plate	$T = T_{amb}$
Condensed mass	Density	Filter paper	$\rho = \rho_{m_0}$
Condensed species	Density	Filter paper	$\rho_m = \rho_{m_0}$ $\rho_{cell} = 0$ $\rho_{ch} = 0$

Table 8. Material data used in the model.

ρ_m (kg/m^3) Density of moist filter paper	491.6	ρ_{cell} (kg/m^3) Density of cellulose (dry filter paper)	491.6	ε_{ch} (1) Emissivity of char	0.95	E_{stell} (GPa) Young's modulus of steel	Eq. 5
ρ_m (kg/m^3) Nonporous density of moist filter paper	1700	$\rho_{s,cell}$ (kg/m^3) Nonporous density of cellulose	1550	ρ_{steel} (kg/m^3) Density of steel	8000	v_{steel} (1) Poisson's ratio of steel	0.25
c_m (J/kgK) Specific heat of moist filter paper	1431	$c_{P\,cell}$ (J/kgK) Specific heat capacity of cellulose	Eq. [6]	$\rho_{s,\,steel}$ (kg/m^3) Nonporous density of steel	8000	α_{steel} (1/K) Coeff. of thermal expansion, steel	$17.8\cdot10^{-6}$
k_m (W/mK) Thermal cond. of moist filter paper	0.164	k_{cell} (W/mK) Thermal conductivity of cellulose	0.136	$c_{P\,steel}$ (J/kgK) Specific heat capacity of steel	500	d_{SP} (µm) Thickness of the steel plate	203
K_m (m^2) Permeability of moist filter paper	$7\cdot10^{-14}$	K_{cell} (m^2) Permeability of cellulose	$7\cdot10^{-14}$	k_{steel} (W/mK) Thermal cond. of steel	Eq. [7]	d_{W2} (µm) Thickness of filter paper	190
ε_m (1) Emissivity of moist filter paper	0.9	ε_{cell} (1) Emissivity of cellulose	0.9	K_{steel} (m^2) Permeability of steel	0	d_{air} (µm) Thickness of the air gap	Eq. 1
ρ_{ch} (kg/m^3) Density of char	111	A_{ev} (1/s) Pre-exponential factor of evaporation reaction	$5.13\cdot10^{10}$	ε_{steel} (1) Emissivity of steel	0.9	v_{cig} (mm/s) Cigarette's burning rate	0.053
$\rho_{s,\,ch}$ (kg/m^3) Nonporous density of char	1500	E_{ev} (kJ/mol) Activation energy of evaporation reaction	88	T_{amb} (K) Ambient temperature	298	P_{qmb} (Pa) Ambient temperature	101300
$c_{P\,ch}$ (J/kgK) Specific heat capacity of char	1300	ΔH_{ev} (J/kg) Heat of evaporation reaction	$2.44\cdot10^{6}$	R (J/mol-K) Universal gas constant	8.314	σ (W/m^{2}K^4) Stefan Boltzmann Constant	$5.6703\cdot10^{-8}$
k_{ch} (W/mK) Thermal conductivity of char	0.105	A_{pyr} (1/s) Pre-exponential factor of pyrolysis reaction	$3.43\cdot10^{17}$	r (mm) Cigarette's radius	8	T_{cig} (K) Cigarette's temperature	Eq. 4
K_{ch} (m^2) Permeability of char	$1\cdot10^{-9}$	E_{pyr} (kJ/mol) Activation energy of pyrolysis reaction	225	ε_{cig} (1) Cigarette's emissivity	0.9	c_{pg} (J/kgK) Specific heat capacity of gases	1000
D_g (m^2/s) Diffusion coefficient of gases	$0.5\cdot10^{-5}$	v_g (m^2/s) Kinematic viscosity of gases	$0.5\cdot10^{-5}$	k_{air} (W/mK) Thermal conductivity of air	Eq. [8]		

where the Young's modulus of the steel:

$$E_{steel} = -1\cdot 10^5 \cdot T^2 + 2\cdot 10^7 \cdot T + 2\cdot 10^{11} \quad [5]$$

the specific heat capacity of the filter paper:

$$c_{P_{cell}} = 1245\cdot\left(\frac{T}{298}\right)^{1.037} \quad [6]$$

the thermal conductivity of the steel

$$\begin{aligned} k_{steel} &= 16.2 && for T < 373K \\ k_{steel} &= \frac{16.2 + (T-373)\times(215-16.2)}{400} && for T > 373K \end{aligned} \quad [7]$$

and the thermal conductivity of the paper

$$k_{air} = 0.026\cdot\left(\frac{T}{298}\right)^{0.845} \quad [8]$$

Numerical implementation

The model was implemented in the commercial finite element method (FEM) software COMSOL Multiphysics, Comsol AB, Stockholm, Sweden. As stated in (3), the finite volume method (FVM) is more convenient for source dominated partial differential equations as those presented in the Table 1. Nevertheless, the implementation of the transient boundary conditions of Table 6 is extremely difficult in most FVM codes, therefore the FEM was used instead. The solution procedure involved an iterative generalized minimal residual solver (GMRES) that sequentially solved the distinct governing equations, i.e., 1) momentum, 2) energy, 3) condensed phase, and 4) condensed phase species. Time step was freely selected by the software, such that stepping was based on instantaneous Péclet number, mesh size and residuals. To improve stability and convergence, density was enforced to be positive, and summation of volume and mass fractions must equal unity. The mesh consisted of about 70,000 tetrahedral elements, which comprised 300,000 unknowns for the CIPT that needed to be determined at each time step. Constant shape functions were used for continuity and species conservation, while linear shape functions were used for temperature and pressure equations. Only half of the substrate was modelled due to symmetry conditions (8), such that the total result could be obtained by mirror reflection respective to the plane containing the contact line between cigarette and substrate. A view of geometry and mesh is presented in Figure 2.

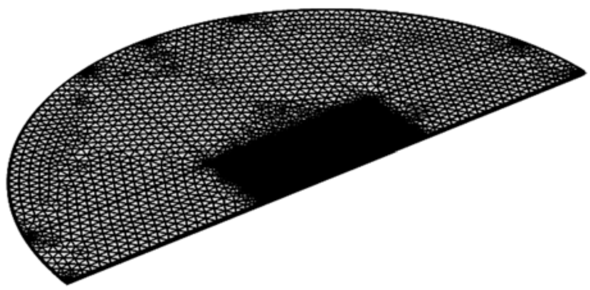

Figure 2. Illustration of the geometry and mesh of the model.

MODEL VALIDTION

As reported in previous research (3, 8), the validation of an IP model must be performed against contactless measurements because the test is extremely sensitive to any contact or manipulation. Thus, the validation consisted of measuring the temperature profile via infrared camera at the lower side of the substrate, which reflects the overall response of the substrate after cigarette's heat absorption (8). Nonetheless, the temperature at the upper side was also measured with the purpose of comparing MIPT and CIPT. Because temperature measurement via IR camera was unfeasible at the lower side of the plate due to brightness, black paint was finely sprayed in order to use the same calibrated emissivity for the whole set of materials. An illustration of the validation layout and typical measurements is shown in Figure 3.

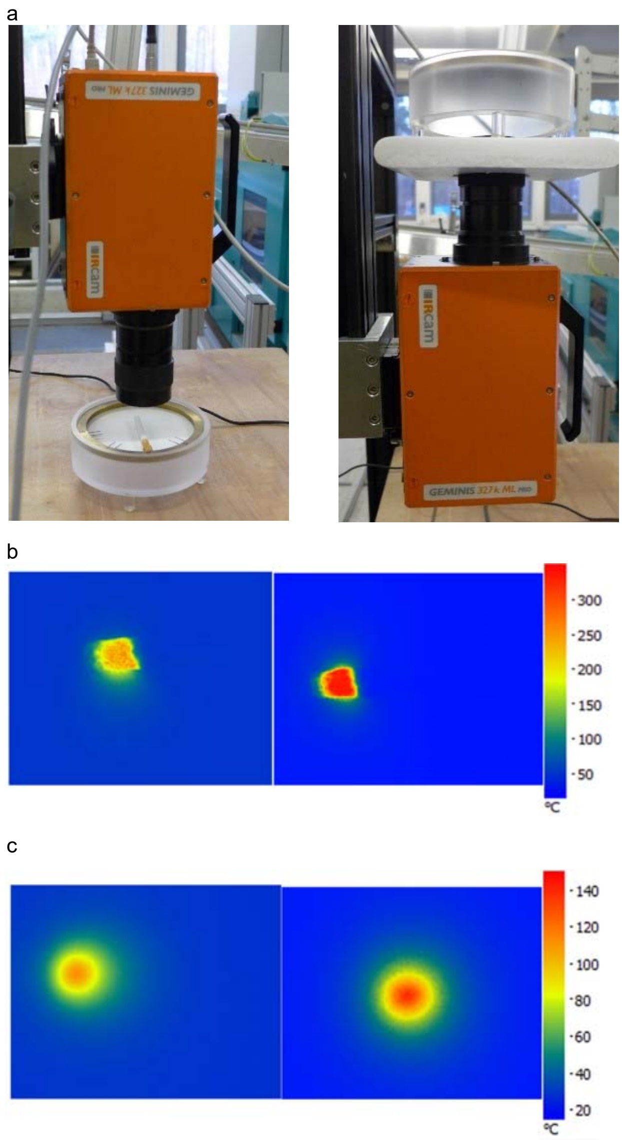

Figure 3. Illustration of the validation set up and experimental measurements. Including: (a) infrared camera layout at the upper and lower side of the substrate; (b) typical temperature measurements at the upper side of a CIPT at the left side and MIPT at the right side; and (c) analogous measurements at the lower side.

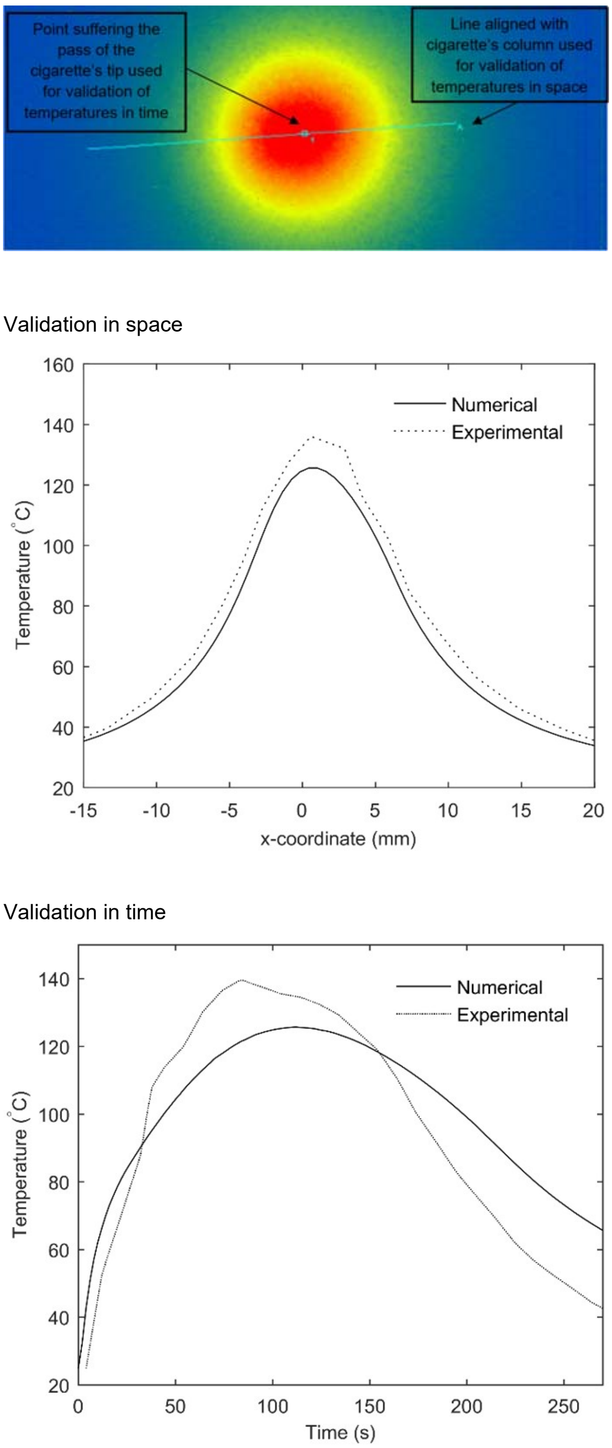

Figure 4. Validation results in predicting the temperature profile at the lower side of the substrate in space and time.

Measurements revealed that, even though the peak temperatures of MIPT and CIPT look similar, two significant differences are noted. First, the gradient of temperature at the upper side of the MIPT is much larger as evidenced by the larger color difference between temperature map of cigarette and substrate. This suggests that MIPT is absorbing the heat much better. Second, the hot area at the lower side of the MIPT is clearly larger than that of the CIPT. Both observations indicate that the substrate in the MIPT is much more thermally conductive than that in the CIPT, and thus in principle the alternative substrate should be prone to absorb more heat from the cigarette.

The validation of the model was performed not only against the temperature profile in space, i.e., the temperature values of the lower side of the substrate along a line aligned with the tobacco column, but also in time, i.e., the temperature wave of a given point of the lower side of the substrate during the pass of the cigarette's smoldering tip. Results indicated that the model was fairly precise in predicting the temperature profile of the substrate, both in space and time, as the computed errors were only 7.3% and 15.7%, respectively, see an illustration of the validation results in Figure 4.

COMPARISON OF HEAT ABSORBANCE

Once the model was validated, the heat absorbance of CIPT and MIPT were compared. In the areas close to the cigarette, the substrate was mostly colder than the cigarette and therefore the heat flux across the substrate's boundaries was positive. Conversely, for most of the areas away from the cigarette the substrate was hotter than the ambient and thus released some heat turning the heat flux negative. The positive heat flux is important, because it actually represents the heat that the substrate is absorbing from the cigarette and as such the release of energy that may cause self-extinguishment. The comparison of the positive heat flux at the upper side of CIPT and MIPT is shown in Figure 5.

The heat flux absorbed by the MIPT was approximately 212% of that from the CIPT as shown in Figure 5. A closer comparison of the temperature isotherms of both tests showed that the hot area of the MIPT was much larger than that of the CIPT, see Figure 6, which means that even when both substrates may have had a priori similar thermal capacities, the substrate in the MIPT was much more conductive and therefore able to absorb the heat much better. This finding is consistent with the experimental measurements obtained with infrared camera presented in Figure 3.

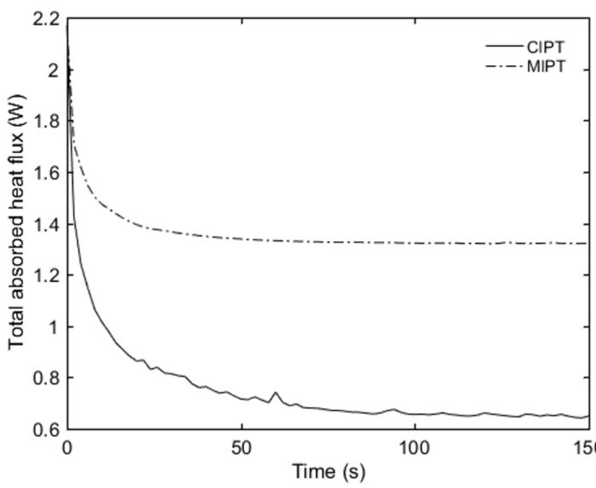

Figure 5. Comparison of heat absorbance from CIPT and MIPT.

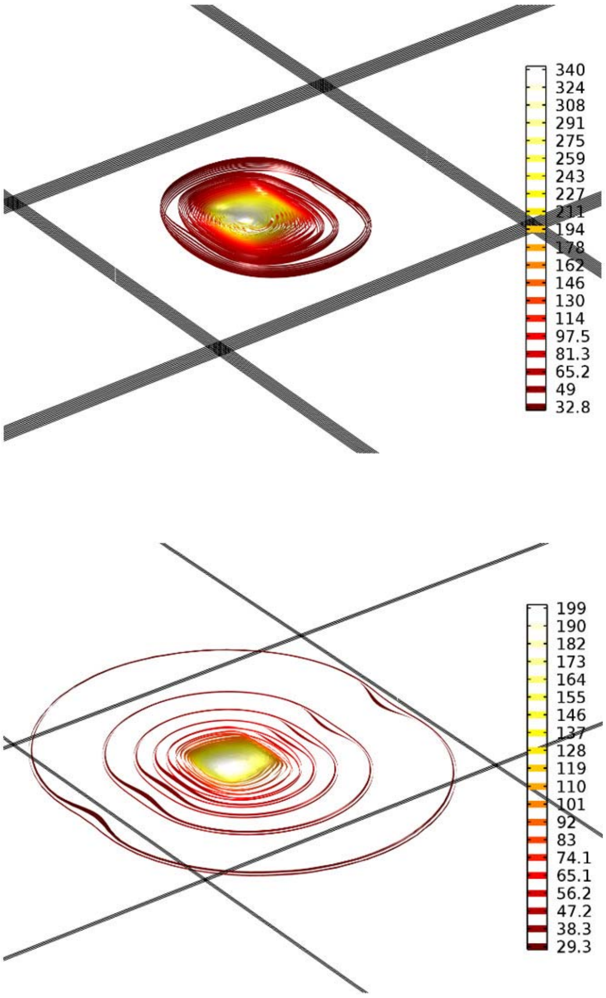

Figure 6. Comparison of the hot areas on CIPT (above) and MIPT (below) by showing the corresponding isotherms of both substrates in Celsius degrees.

ANALYSIS AND DISCUSSION OF POTENTIAL VARIABILITY

The overall variability of the MIPT can be seen as caused by the filter paper plus that of the metal plate. As the variability concerning the filter paper has been presented elsewhere (3), this section is focused on analysing the potential variability caused by the stainless steel.

Tolerance of steel plate manufacturing

ASTM E2187-16 prescribes a plate with a thickness of 0.203 mm ± 0.004 mm. Based on the results of an experimental investigation of three major steel manufacturers (10), those with ± 0.004 mm would imply a discard rate of about 20% of the samples. Computations of the heat absorbed by MIPT with plates of 0.199 mm and 0.207 mm in thickness showed that there is virtually no difference. Thus, the variation expected due to the manufacturing tolerance was negligible.

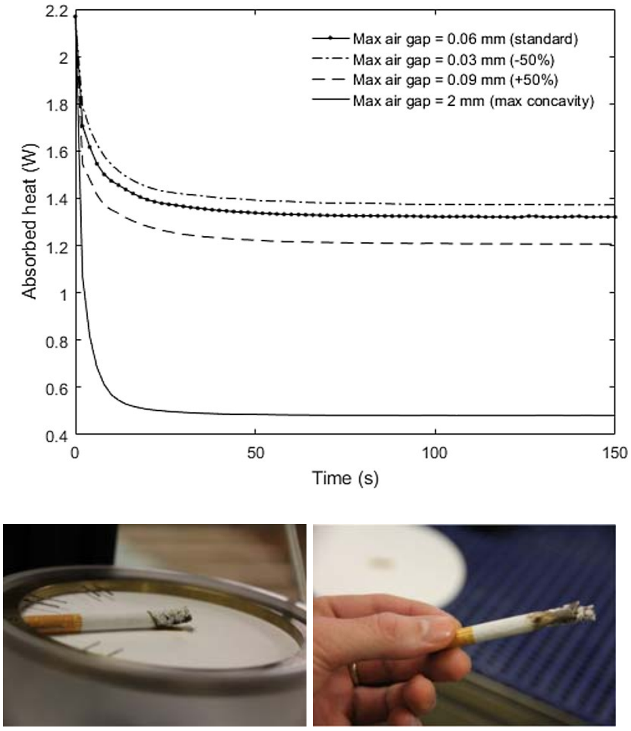

Figure 7. Variability on the heat absorbed by the substrate during MIPT: (above) numerical results due to potential variations of air gap thickness; (below) visible plate concavity and consequent smoldering irregularities after some testing.

Air gap thickness

As previously introduced, the expected variability caused by the measured air gap in a CIPT is much higher than that of the MIPT because the latter involves a single air gap layer. Actually, the numerical results indicate that varying the air gap thickness of about ± 50% would only imply a 4% change in the heat absorbed by the substrate in a MIPT, as seen in Figure 7. This variability is clearly lower than expected as compared to the CIPT, where changes of heat absorbance due to ± 50% of air gap were reported as high as 33% (3).

Potential deformations of the metal plate

Three nonlinear mechanical phenomena might occur in steel during MIPT: (i) Buckling: When thin sheets of steel are subjected to significant compressive stresses, they tend to buckle. The buckling of steel would significantly increase the air gap thickness causing plate concavity; (ii) Plasticity: Steel yield limit (onset for plastic deformations) strongly decreases at high temperatures (13), meaning that permanent deformations are much more likely in hot steel. In that case, deformations cannot be recovered after cooling, and the plate would progressively deform in consecutive tests; (iii) Creep: When subjected to constant loading (gravity), steel tends to increase the deformation with time, and this phenomenon is significant at high temperatures (13).
In order to assess the risk of these nonlinear phenomena in increasing steel plate deformations (and thus air gap), a mechanical analysis was performed based on the properties

presented in Table 8. Note that the steel undergoes deformations when heated as per the thermal expansion coefficient. Thus, when the temperature rises in the central hot region of the plate, it expands. The peripheral region of the plate however is colder and does not expand, therefore it constrains the deformation of the central region, causing a significant compressive loading in the centre of the plate. The mechanical implementation was performed in the numerical model as detailed below. Displacements were found by imposing the divergence of stress tensor

$$\nabla\sigma + F_V = 0 \quad [9]$$

Strains were then computed form displacements as

$$\varepsilon = \frac{1}{2}\left[\nabla u^T + \nabla u\right] \quad [10]$$

On the other hand, thermal induced strains are computed using the temperatures of the thermodynamical analysis and thermal expansion coefficient as

$$\varepsilon_{th} = \alpha\left(T - T_{ref}\right) \quad [11]$$

So the elastic strains can be calculated

$$\varepsilon_{el} = \varepsilon - \varepsilon_{th} \quad [12]$$

To finally compute stress by applying the constitutive relationship

$$\sigma = C \div \varepsilon_{el} \quad [13]$$

with

$$C = \frac{E_{steel}}{(1+v)\cdot(1-2v)}\begin{pmatrix} 1-v & v & v & 0 & 0 & 0 \\ v & 1-v & v & 0 & 0 & 0 \\ v & v & 1-v & 0 & 0 & 0 \\ 0 & 0 & 0 & 1-2v & 0 & 0 \\ 0 & 0 & 0 & 0 & 1-2v & 0 \\ 0 & 0 & 0 & 0 & 0 & 1-2v \end{pmatrix} \quad [14]$$

being the Poisson's ratio $v = 0.25$.

After mechanical computation, it was found that actually the compressive stress in the central part of the plate was close to the steel yield limit, see Figure 8. This indicates that risk is very high for buckling, yielding and creep to affect the steel plate. All these phenomena have the potential to modify the air gap significantly by progressively and irreversibly increasing plate deformation.
During the experiments, it was found that even when the plates were allowed to fully cool after MIPT, concavity of the steel was increasing with subsequent tests. This caused not only a visible increase of the air gap, but also hampered the contact of the cigarette with the substrate in the central region due to concavity, see an illustration of a cigarette during and after MIPT in Figure 7. Such concavity is has a decisive influence for the reliability of the MIPT.
The ASTM E2187-16 states that concavity should not exceed 2 mm in any part of the plate. However, numerical

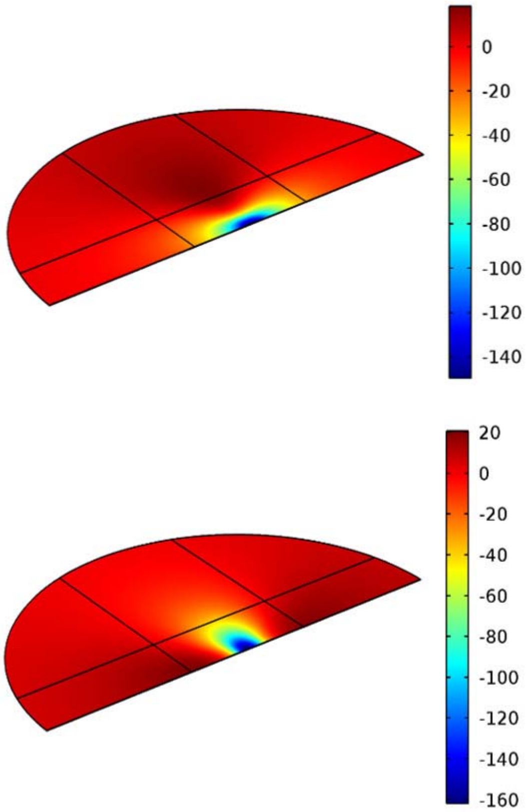

Figure 8. Mechanical analysis shows that stress at the central part of the plate is close to yield due to high temperature gradients. Above figure shows mechanical stress in MPa along cigarette direction, and below figure shows stress perpendicular to the cigarette direction.

results showed that a 2 mm air gap in between filter paper and steel plate reduces the heat absorbance by 62%, which is problematic. In addition to the effect of an increasing air gap, the concavity of the substrate reduces the intensity of the contact with the cigarette, so that in reality the effect of concaveness on heat absorbance is deemed much higher than 62%.

Rectangular or circular-shaped steel plates

The potential effect of having a rectangular plate of comparable size was computed in order to compare its heat absorbance with respect to a circular plate. Results indicated that there was no difference of using a rectangular plate because the temperatures at the periphery were mostly as low as the ambient and thus the heat flux at the periphery was negligible.

CONCLUSION

A detailed experimental and theoretical analysis of the new alternative ignition propensity test based on the utilization of a thin stainless steel plate was conducted in this investigation. The theoretical analysis was based on a detailed and accurate computational model that considered the most important thermophysical phenomena. It was validated experimentally with full-field infrared temperature measurements serving to prove the accuracy of current computational models.

The alternative test substitutes the nine lowermost filter paper layers of the traditional test procedure by steel, which compared to filter paper is a homogeneous, non-charring and airtight material. Although in principle the wide availability, homogeneity, manufacturing accuracy and reusability of steel could make this test very attractive, a number of critical downsides were found, both experimentally and theoretically:

- Heat absorbance is largely underestimated. For a flat steel plate, the heat absorbance was more than twice the absorbance of the substrate used in the conventional test due to the high thermal conductivity of steel.
- Filter paper and air gap variability still play a crucial role because the test avoids neither the use of Whatman® paper No. 2 nor the usage of two different layers.
- Plate deformations and air gaps proved to be less controllable than in the conventional test. In addition to the deformation of the filter paper, the steel plate could suffer much larger deformations thus varying the air gap thickness drastically and with that the substrate's heat absorbance. These deformations may not only be caused by gravity but also due to multiple mechanical risks such as buckling, yielding and creep of the plate. This is crucial considering that all these phenomena are more critical at high temperatures, and they are not reversible. While ASTM E2187-16 limits the deformation of the plates to 2 mm, both the experiments and the theoretical model revealed that this deformation is unacceptable because heat absorbance is halved in comparison with the case of a perfectly flat plate and also that the contact between substrate and cigarette is visibly modified.

All these observations suggest that the new method does not correctly reproduce the thermodynamics of the conventional method and is less reliable. Therefore, the utilization of the conventional ignition propensity test is recommended until a more reliable method is proposed.

ACKNOWLEDGMENTS

This research was funded by the German Cigarette Association and the authors are grateful for the support.

REFERENCES

1. American Society of Testing Materials (ASTM) American Standard 2187-16. Standard Test Method for Measuring the Ignition Strength of Cigarettes; ASTM, West Conshohocken, PA, USA, 2016.
2. International Organization of Standardization (ISO): International Standard 12863:2010. Standard Test Method for Assessing the Ignition Propensity of Cigarettes; ISO, Geneva, Switzerland, 2010.
3. Guindos, P., A. Patel, T. Kolb, P. Meinlschmidt, F. Schlüter, and B. Plinke: Experimental and Numerical Characterization of the Influence of a Smoldering Cellulosic Substrate on a Cigarette's Ignition Propensity Test; Fire Technology (Accepted for publication) (2018).
4. Gann, R.G. and W.F. Guthrie: Robustness of Measuring the Ignition Strength of Cigarettes With ASTM Method E2187-02b; NIST TN 1454 (2003).
5. Su, J.Z., P. Leroux, and J.C. Latour: Cigarette Ignition Propensity Testing: First Series; Institute for Research in Construction, National Research Council Canada (2003).
6. Gann, R.G.: Measuring the Ignition Propensity of Cigarettes; *in:* Proceedings of the Interflam Fire Science and Engineering Conference (2007) pp. 145–55, London, UK.
7. Mehta, S.: Cigarette Ignition Risk Project; U.S. Consumer Product Safety Commission, Maryland , US, 2012.
8. Guindos, P., C. Michel, and C. Weichert: Numerical Model to Quantify the Influence of the Cellulosic Substrate on the Ignition Propensity Tests; Beitr. Tabakforsch. Int. 27 (2016) 102–112.
9. Mitler, H.E. and G.N. Walton: Modeling the Iignition of Soft Furnishings by a Cigarette; US Department of Commerce, National Institute of Standards and Technology, 1993.
10. Gann, R.G., M.C. Bruns, E.J. Hnetkovsky, and W.F. Guthrie: Interlaboratory Study of an Alternate Substrate for Use in ASTM 2187. NIST Technical Note 1874 (2016).
11. Baker, R.: Temperature Variation Within a cigarette Combustion Coal During the Smoking Cycle; High Temp. Sci. 7 (1975) 184–224.
12. MatWeb, LLC: MatWeb™ Materials Database; http://www.matweb.com/ (accessed August 2018), Blacksburg, VA, USA.
13. American Iron and Steel Institute: A Designer's Handbook Series N°9004: High Temperature Characteristics of Stainless Steel. Washington, DC, USA, 2002.

Corresponding author:

Pablo Guindos, PhD
Pontificia Universidad Católica de Chile
Vicuña Mackenna 4860
7820436 Santiago, Chile
E-mail: pguindos@ing.puc.cl